Technical Note

Fracture and Fatigue Design of the Wilshire Grand Tower

AMIT KANVINDE, PETER MARANIAN, LEONARD JOSEPH and JEFF LUBBERTS

ABSTRACT

The 1,100-foot Wilshire Grand Tower in Los Angeles owned by the Hanjin Group is the tallest building in the United States west of Chicago. The building, whose architect is AC Martin Inc., has a slender elevation in one direction, necessitating the use of heavy steel box columns filled with concrete on the perimeter, connected to the concrete core with outrigger trusses. The building has a slender, 272-ft-tall spire, also constructed from steel plates. The height and slenderness of the tower, as well as the spire, and its location in a seismically active zone motivated comprehensive analysis to mitigate the risk of steel fracture within a performance-based design framework. This analysis includes the following components: (1) development of acceptance criteria for earthquake-induced fracture, especially when it may follow years of wind-induced fatigue crack growth; (2) wind tunnel testing; (3) linear and nonlinear time-history simulations to determine stress demands in critical components under appropriate wind and seismic hazards; and (4) fracture mechanics simulations to characterize trade-offs among various design variables to meet the acceptance criteria. The analysis indicates that wind-induced oscillations have the potential to grow fatigue cracks in some components, affecting their performance during a subsequent maximum considered earthquake. This situation is unusual for steel buildings, being the result of the extraordinary height, geometry, heavy steel members, and location of this particular building. The analysis also indicates that fracture risk may be successfully mitigated through existing design and detailing approaches and acceptance criteria, along with use of steel material exhibiting high, but commercially available and affordable, specified Charpy V-notch toughness values.

Keywords: fracture, fatigue, tall buildings.

INTRODUCTION

The landmark 1,100-ft, 73-story Wilshire Grand Tower in Los Angeles (completed in 2017; see Figure 1), the tallest building in the United States west of Chicago, features innovative engineering in steel design and construction. Located in a seismically active zone, its lateral load-resisting concrete core and steel outrigger system has attracted public interest, with articles in the *Los Angeles Times* (Curwen, 2014), *Structure Magazine* (Nieblas, 2014), and *Civil Engineering* (Joseph and Maranian, 2017). The building is exceptional due to its height, complex shape, and narrow floor plan, resulting in a slender elevation, along with its prominence as the tallest building in the western United States. Very heavy steel members (including built-up box sections) with complex connections were required to resist large forces accompanied by cyclic responses, both earthquake- and wind-induced, during its anticipated life span. The structural design team determined that this warranted consideration of effects beyond code as well as the performance-based design (PBD) procedures and criteria approved by the building department and its peer review panel. The goal was to mitigate the risk of steel fractures in framing, including column-foundation connections, column splices, outrigger elements, along with their connections, and the spire components and connections.

Specific criteria and procedures, using sophisticated simulations and probabilistic representations of seismic and wind hazards, were implemented for this building within a PBD framework (ATC, 2010, 2012). Special analyses were performed to predict and address structural fracture and fatigue demands within the design of the tower's framing system and spire, based on the anticipated demands during the expected life of the building. The primary objectives of this paper are (1) to provide an overview of unique fracture and fatigue issues faced by supertall and slender buildings constructed with heavy steel subject to seismic and wind hazards and (2) to provide guidance for mitigating these issues within the framework of current technology, industry standards, and professional practice.

Amit Kanvinde, Professor, Department of Civil and Environmental Engineering, University of California, Davis, CA. Email: kanvinde@ucdavis.edu (corresponding)

Peter Maranian, Principal, Brandow & Johnston Inc., Los Angeles, CA. Email: pmaranian@bjsce.com

Leonard Joseph, Principal, Thornton Tomasetti, Inc., Los Angeles, CA. Email: LJoseph@thorntontomasetti.com

Jeffrey Lubberts, P.E., S.E., Associate Principal, RGSE Inc., Simi Valley, CA. Email: jeffl@rgseinc.com

Paper No. 2017-10

The paper begins by presenting an overview of the structural system and spire of the building, identifying regions that were studied for fracture resistance. Approaches used for simulation of wind and seismic hazards are then outlined; this is followed by a discussion of the methods used to simulate wind-induced fatigue followed by earthquake-induced fracture. The paper concludes by summarizing the effect of these studies on design decisions, along with broader implications for fracture assessment of special structures similar to the Wilshire Grand Center Tower.

STRUCTURAL SYSTEM AND SPIRE

The structural system, shown in Figure 2, is designed to be stiff for occupant comfort under service level wind loads while providing sufficient strength to resist seismic loads generated by this stiffness. Floor slabs on steel beams are supported by a concrete core and perimeter concrete-filled steel box columns. To suit the tower floor plan, the central core is narrow, with a roughly 4:1 plan aspect ratio. To improve building performance (i.e., control forces and deformations) in the transverse or "weak" direction, multistory outrigger trusses connect core walls to perimeter columns at three levels. Atop the concrete core a trussed steel "sail" feature rises 100 ft. Tied to it is a 272-ft-tall spire consisting of a shell of brake-bent steel plates. The shell tapers from 6.5 ft to 2.7 ft in diameter. Each 40-ft segment of the spire has a constant plate thickness, with field-bolted end plate splices sized to avoid prying action. These elements of the structure are identified in Figure 2, along with steel connections and components subjected to special attention with respect to fracture: (1) complete-joint-penetration (CJP) connections from box column to cap plate on "starter columns" in the foundation, Figure 2(a); (2) field splices of box columns incorporating partial-joint-penetration (PJP) welds, Figure 2(b) (these welds contain an external flaw that increases fracture toughness demand); (3) starter column cap plates, as well as bolted end-plates in the spire with through thickness demands at the CJP welds, which involved reinforcing fillet welds, Figure 2(c); and (4) spire shell plates, Figure 2(d). Demands in these connections arise from both wind and seismic effects. For both the tower and the spire, wind-tunnel studies showed that vortex-induced oscillations occur in multiple modes (at different wind speeds) and generate cyclic stresses at connections. Wind-induced cyclic stresses are well below steel yield but not low enough to discount the possibility of fatigue crack growth from a large number (~10^6) of cycles (high cycle fatigue). Conversely, seismic demands, especially at the maximum considered earthquake (MCE) level, induce stresses on the order of the yield stress, but with only a few (~10–20) cycles (ultra-low cycle fatigue).

Fig. 1. The Wilshire Grand Tower in downtown Los Angeles (rendering).

The next section summarizes the simulation of demands; these are in the form of stress ranges and cycles for wind loading and peak stresses for earthquake loading.

SIMULATION OF WIND AND SEISMIC EFFECTS WITHIN A PERFORMANCE-BASED DESIGN FRAMEWORK

Key to PBD is probabilistic simulation of natural hazard effects (wind, earthquake) and setting of target structural performance objectives or acceptance criteria under these hazards. As for most buildings, wind-induced fatigue in itself is not a controlling limit state for the Wilshire Grand Tower. However, wind tunnel studies of both tower and spire (in conjunction with structural simulations) indicated the potential for wind-induced oscillations capable of causing fatigue crack extension in critical components, increasing the vulnerability under a late-in-life major seismic event. Acceptance criteria for this newly plausible wind followed by earthquake scenario are not established, in contrast to those that do exist for purely seismic limit states (see, e.g., ATC, 2010). As a result, new acceptance criteria were developed specifically for this project. For elements of the tower itself, the performance objective was to prevent fracture, or to have a negligible probability of its occurrence, in the scenario of the MCE earthquake occurring even after 100 years

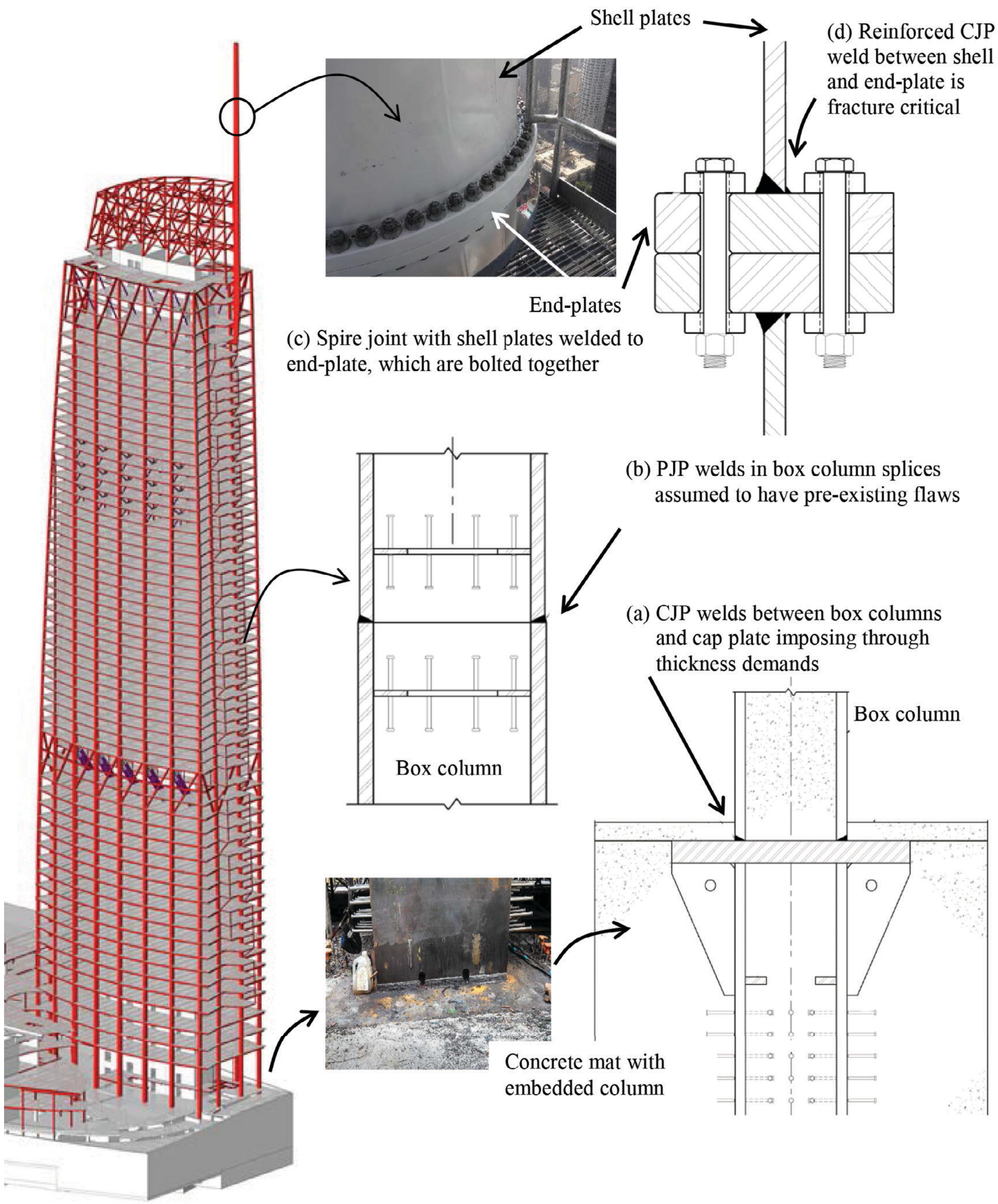

Fig. 2. Selected fracture critical details in the tower and spire.

of wind fatigue accumulation. For elements of the spire, an MCE event after a 50-year wind exposure window was selected.

Simulation of Wind Effects

To meet the acceptance criteria previously outlined, it is necessary to estimate fatigue crack growth during the time windows of interest—that is, 100 and 50 years for the tower and spire, respectively. This entails characterization of the stress cycles (both the stress ranges as well as the number of cycles in each range) due to wind-induced oscillations. The effect of wind-induced oscillations on the tower and spire was assessed through wind tunnel testing conducted on 1/400 and 1/60 scale models, respectively, by Rowan Williams Davies and Irwin (RWDI) Inc. Figures 3(a) and 3(b) show photographs of the tower and spire being subjected to wind loads. The tower study used a "rigid-building" wind tunnel model, where aero-elastic interactions between the model and the wind flow were disregarded (as is often the practice). Building deformations were not measured, while the base moments were. The spire study used an aero-elastic model focusing on the first three vibration modes. Specifically, the wind tunnel tests and associated modeling included the following tasks:

1. A statistical wind climate model was developed for the site based on wind data measured at Los Angeles International Airport. This model includes mean annual frequencies of exceedance of wind speeds, including the effects of directionality. This model may be used to determine the duration the building spends in each wind regime (i.e., combination of direction and wind speed) over a given time window.
2. For each plausible wind regime, wind tunnel testing was used to record building oscillations, which are irregular and complex in form. These were subsequently converted to equivalent sets of constant range cycles; this included characterization of mean and range quantities (such as base moment along each axis of the building), along with cycle counts (determined per hour).
3. The wind tunnel data generated in this manner were used in conjunction with structural models to determine stress history information (i.e., mean stress, stress-range, and cycles per hour) at the component level corresponding to each wind regime. The mean stress, along with the stress ranges, may be used to determine the "stress ratio" for each set of cycles; this is subsequently used in the calculation of a threshold stress range above which fatigue cracks tend to grow.
4. The final step involved integrating these data with the wind climate model (point 1) to determine stress cycle data at each critical component (i.e., the components in Figure 2) over the time window of interest. Table 1 provides a sample of such data, which are used (as discussed in a subsequent section) to estimate fatigue crack growth.

Simulation of Seismic Effects

Nonlinear response history analysis (NLRHA) simulated both geometric and material nonlinearity in the structure. For MCE-level motions (2,475-year mean recurrence interval), multiple time-history suites were rigorously selected through a peer review process to address both M7.8 strike slip events on the distant San Andreas fault and M6.6 events on a reverse or reverse-oblique local fault—for example, the Puente Hills Blind Thrust Fault. Based on the NLRHA,

(a) (b)

Fig. 3. Wind tunnel model of (a) tower and (b) spire.

Table 1. Sample Table Showing Stress Cycle Data		
Stress Range $\Delta\sigma$, ksi	**Number of Cycles, N**	**Mean Stress, ksi**
6.3	565330	4.41
8.4	90190	5.88
10.5	17208	7.35
12.6	3423	8.82
…	…	…
..	..	..

the peak stresses were recorded for all critical components, including those identified previously in Figure 2. The simulations indicate that although none of the fracture critical components studied would have significant inelastic deformation, stresses in some components approach the yield strength. Note that components designed to be dissipative (e.g., the buckling restrained braces) are not fracture critical due to special detailing, except where their gusset plates are welded to large embedded plates in the core walls. In these cases, welding requirements followed those used at the connections from box columns to cap plate at the starter columns.

Simulation of Fatigue Crack Growth Followed by Fracture

The well-known Paris's fatigue law (Paris and Erdogan, 1963) was used to estimate fatigue crack growth in the components of interest. Paris's law, commonly used for fatigue assessment of mechanical and aerospace components, relates the rate of crack growth per stress cycle to the stress range (given the presence of a crack or flaw). Equation 1 expresses Paris's law mathematically, whereas Figure 4 illustrates the associated quantities and process for the

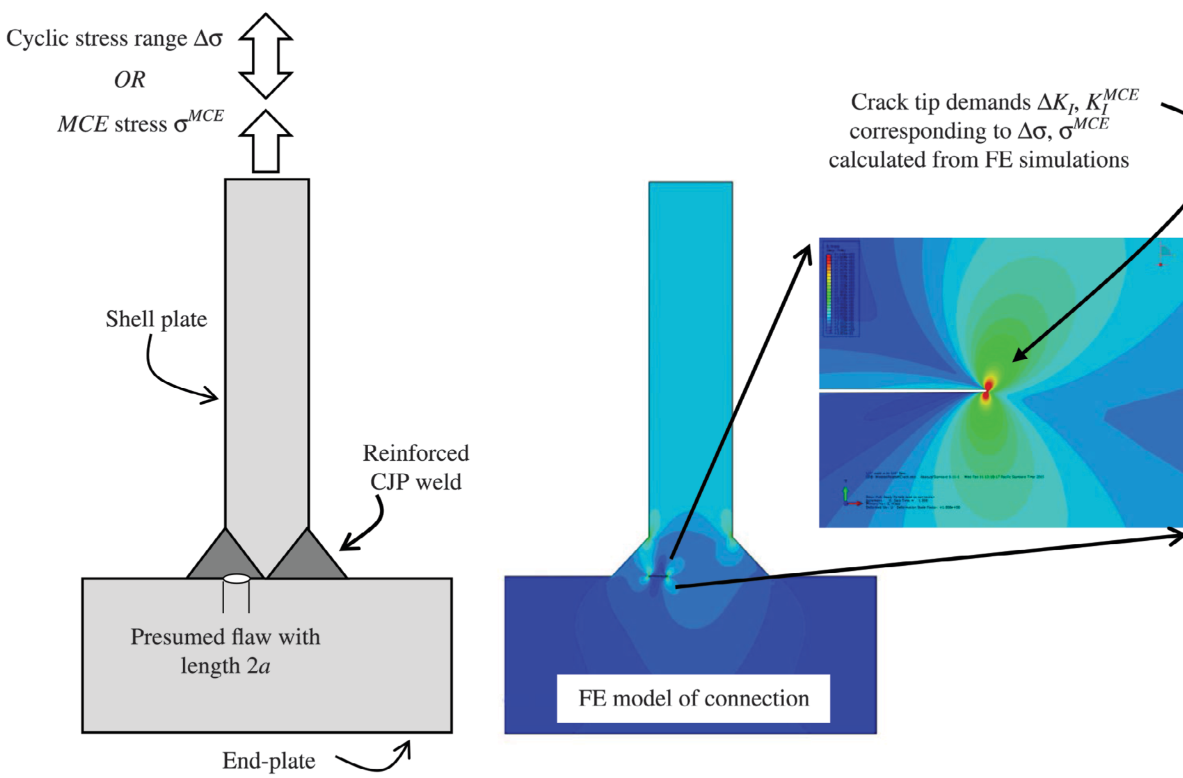

Fig. 4. Finite element model of spire connection (shown previously in Fig. 2) to determine crack tip conditions for fatigue crack growth and fracture.

shell-plate to end-plate connection in the spire shown previously in Figure 2(d).

$$\frac{da}{dN} = C(\Delta K_I)^m \text{ for } \Delta K_I \geq \Delta K_{I\text{-}thresh}; \tag{1}$$

$$\frac{da}{dN} = 0 \text{ for } \Delta K_I < \Delta K_{I\text{-}thresh}$$

In Equation 1, da/dN denotes the rate of crack growth with respect to the number of cycles (a denotes crack length; N denotes number of cycles), whereas ΔK_I represents the range of the stress intensity factor K_I (in which the subscript I refers to mode I or crack opening), corresponding to the range of applied stress, $\Delta\sigma$ (see Figure 4). The terms C, m and $\Delta K_{I\text{-}thresh}$ are material parameters. Of these, the first two are taken as 3.6×10^{-10} and 3.0, respectively, for structural steel, whereas the threshold value $\Delta K_{I\text{-}thresh}$ depends on the ratio of minimum to maximum stress within the stress range (Barsom and Rolfe, 1999). The stress intensity factor (Anderson, 1995) relates remotely applied stresses to the crack tip stress field through relationships involving the crack length and specimen geometry. Equation 2 expresses such a relationship:

$$\Delta K_I = (\Delta\sigma)\alpha\sqrt{\pi a} \tag{2}$$

The factor α is geometry dependent and may be determined through finite element simulation or analytical expressions (e.g., Rooke and Cartwright, 1976). For critical components in the tower and spire, the law was applied in the following manner:

1. An initial flaw was assumed in the component. The shape and size of this flaw were based on the specific detail, the way the flaw would be introduced (weld lack-of-fusion, material inclusion), and the resolution and acceptance criteria of ultrasonic testing for flaw detection. For example, Figure 4 illustrates a possible lack-of-fusion flaw in the CJP weld. Various initial flaw dimensions and locations were tested to inform design trade-offs against inspection criteria.

2. The stress-cycle ranges for each component and time window (as shown previously in sample Table 1) were interpreted through Paris's fatigue law to determine growth of the assumed flaw, by integrating Equation 1. Note that the integrand of the equation contains ΔK_I, which itself is a function of the evolving crack length as expressed in Equation 2. Consequently, the integration is performed numerically by discretizing the cycle groups in Table 1 into smaller bins. The cycle groups are applied in various orders (decreasing, increasing, or random amplitude sequences) to determine the sequence that results in the greatest crack growth at the end of the time window; this crack length is denoted as $a_{fatigue}$.

3. Once wind-induced fatigue crack growth at the end of the time window was determined for each component, fracture mechanics analyses were conducted to determine the toughness requirements to meet demands under MCE level stresses. In cases where crack tip yielding was expected to be limited (either due to geometry or lower MCE stresses), linear elastic fracture mechanics was used, including application of the stress intensity factor K_I^{MCE} to find MCE-level demands for establishing required toughness. When significant crack tip yielding was expected, elastic plastic fracture mechanics was used, relying on the J-integral as the fracture toughness demand (Rice, 1968). In many cases, where expressions relating K_I^{MCE} to σ^{MCE} were available in literature (Anderson, 1995) or in compendia of stress-intensity factor solutions (Rooke and Cartwright, 1976), K_I^{MCE} could be determined conveniently in a manner similar to ΔK_I for fatigue stresses, by using MCE-level stresses and the length of the fatigue crack (as computed previously). Specifically,

$$K_I^{MCE} = \sigma^{MCE}\alpha\sqrt{\pi a_{fatigue}} \tag{3}$$

In some situations (e.g., CJP welded joints in the spire with reinforcing fillet welds; see Figure 2), such expressions were not available. In these cases, or when crack tip plasticity was expected, continuum finite element simulations (such as the one shown in Figure 4 for the joint previously shown in Figure 2) were used to determine fracture toughness demands. These simulations also included the effects of welding-induced residual stresses on the computed fracture toughness demands.

4. The fracture toughness capacity K_{IC} is not usually specified or measured for structural steel used in seismic construction because professional practice (including the 2016 AISC *Seismic Provisions*) relies on having material with minimum Charpy V-notch (CVN) energy measured at specific temperatures that is, 20 ft-lb at and 40 ft-lb at 70°F from heat input envelope testing. Barsom and Rolfe (1969) provide a convenient correlation between the CVN energy and a dynamic fracture toughness value K_{ID}, as shown in Equation 4:

$$K_{ID} = 0.001\sqrt{(0.005\text{CVN})E} \tag{4}$$

where K_{ID} represents the dynamic fracture toughness (in the units of ksi$\sqrt{\text{in.}}$), which is associated with the high strain rate of a Charpy energy test, while E is the modulus of elasticity in ksi, and CVN is the measured energy in ft-lb. However, strain rates during seismic events are significantly lower (on the order of 0.01–0.1 strain/second, as compared to 1–1000 strain/second for Charpy specimens; see Lei et al., 1993). It is well known (Barsom and Rolfe, 1999) that high strain rates reduce fracture toughness. To resolve this, the dynamic toughness K_{ID} may be reinterpreted as the available toughness at a lower temperature, through a "temperature shift," which depends on the strain rate (Barsom and Rolfe, 1999). For the Wilshire Grand Tower and spire, this implies that K_{ID}, as determined through Equation 4, using dynamic CVN measurements at 70°F provides a conservative estimate of fracture toughness under seismic loading rates for service temperatures above 35°F. This difference (35°F) is greater than the difference (20°F) implied by the AISC *Seismic Provisions* (AISC, 2016), which assumes a LAST (lowest anticipated service temperature) of 50°F.

Once both the toughness demand and capacity are thus established, they may be compared to assess the safety of a given component and guide design refinements to meet acceptance criteria. The next section describes this process.

EFFECT ON DESIGN DECISIONS

For each fracture critical component, the process just described was conducted with various trial input variables to meet the acceptance criteria (i.e., toughness demands less than capacity for MCE stresses after 50 or 100 years of fatigue crack growth). Figure 5 shows a representative graph summarizing the results of this type of analysis for one such component, the connection in the spire shell plate shown earlier in Figure 4. The figure indicates that acceptance criteria can be achieved through a combination of three variables: (1) providing adequate material fracture toughness—that is, the specified CVN value(s); (2) controlling stresses within the component by increasing weld sizing/reinforcing fillets where needed; and (3) restricting the initial flaw size based on the detection techniques used and their precision. In this context, it is relevant to note that AWS D1.1 (2010) was used for quality control and quality assurance with requirements similar to AWS D1.8 (2009) noted on the drawings. All complete penetration welds and some partial penetration welds were tested by ultrasonic testing, and magnetic particle testing was carried out on some of the partial penetration welds and fillet welds. During construction, reinspection—including visual, magnetic particle, and ultrasonic testing—was carried out to check for possible delayed cracking.

Figure 5 shows that the consequences of larger permissible initial flaw size may be mitigated through either tougher material or a thicker shell plate. With the knowledge of such trade-offs, each of these design variables may be controlled within the constraints of available materials, technology and cost to obtain acceptable performance. In some locations, this approach involved specifying higher material toughness than mandated by existing standards, for example:

1. The cap plates on the starter columns [Figure (2a)], as well as other similar plates, subjected to through thickness demands, required a CVN of 59 ft-lb at 70°F in the through-thickness direction. CVN tests were carried out in the weld material and the heat affected zone (HAZ). The steel material required a yield ratio less than 0.85.

2. Welding procedure specifications for complete penetration welds, with connection plate subject to through-thickness loading, required testing per ASTM 770 (2012), with a 25% minimum reduction required in weld material and the HAZ.

3. The spire end plates, subjected to through-thickness loading, required CVN testing of 20 ft-lb at 70°F in the

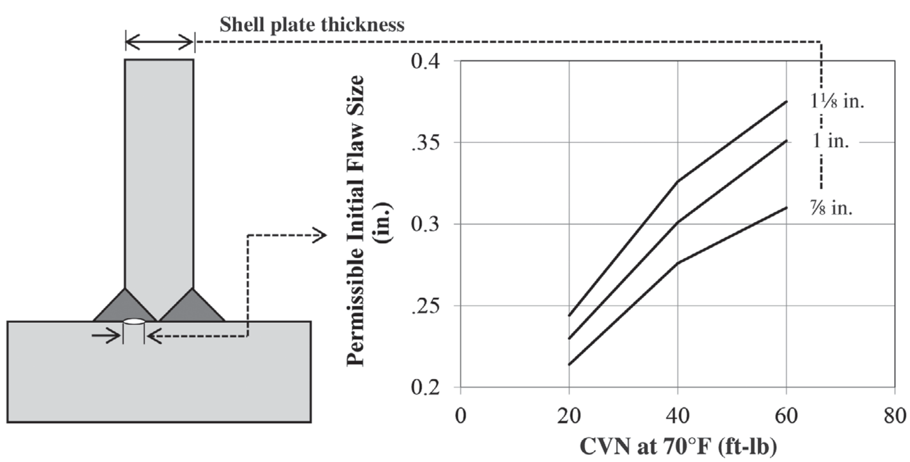

Fig. 5. Finite element model of spire connection (shown previously in Figs. 2 and 4) to determine crack tip conditions for fatigue crack growth and fracture.

through-thickness direction. Similar to cap plates on the starter columns, CVN testing was performed on the weld material and HAZ. The steel material required a yield ratio < 85%.

4. Welding procedure specifications for the spire shell plate to flange plate complete penetration welds, which included reinforcing fillet welds, required testing per ASTM 770 (2012) with a 25% minimum reduction required in weld material and HAZ.

In other situations, such as buckling restrained brace (BRB) gusset plates welded to large embedded plates in the core walls, toughness was specified and tested in the through-thickness direction of the plate, which is not typically done (e.g., the base plate shown previously in Figure 2). Finally, at all regions where fracture was a possibility, ultrasonic testing was specified on base metal subjected to through-thickness stresses, and on complete penetration welds, to detect and limit flaws to within acceptable sizes.

SUMMARY

As a landmark steel building in Los Angeles, the Wilshire Grand Tower received project-specific fracture analysis with a degree of sophistication rarely used before in the building construction industry. The analysis was suited to the PBD approach used for the building's design and its location in a seismically active region. Key findings were that wind-induced oscillations have the potential to grow preexisting flaws in the building over its lifetime and that consideration of this flaw growth is warranted while examining performance under MCE level seismic shaking.

As climatological hazards evolve, this type of multi-hazard interaction may become commonplace, and the analysis described here provides a rational methodology to assess risk under such interacting hazards. It is interesting to note that the findings, using this methodology, naturally extend the industry direction (motivated by the 1994 Northridge earthquake) toward improvements in material toughness, detailing, and material requirements. Stringent performance objectives can successfully be achieved through existing design and detailing approaches and acceptance criteria, along with steel having higher-than-typical, but commercially available and affordable specified CVN values. This is very helpful for using steel in large structures in highly seismic regions that can be subjected to wind-cyclic fatigue loading. In fact, the analysis procedures and risk mitigation measures, outlined in this study, are enabled by a confluence of two key factors: (1) increased awareness of fracture in steel structures and strategies for mitigation, after the Northridge earthquake, and (2) maturation of PBD methodologies, facilitated by landmark documents such as FEMA P-58 (ATC, 2012) and ASCE 41 (2014). In this broader context, the procedures established for this project should continue to be researched and developed further for use in similar special structures.

REFERENCES

AISC (2016), *Seismic Provisions for Structural Steel Buildings*, ANSI/AISC 341-16, American Institute of Steel Construction, Chicago, IL.

ASCE (2014), *Seismic Evaluation and Retrofit of Existing Buildings*, ASCE 41-13, American Society of Civil Engineers, Reston, VA.

ATC (2010), *Modeling and Acceptance Criteria for Seismic Design and Analysis of Tall Buildings,* ATC-72-1, Applied Technology Council, Redwood City, CA.

ATC (2012), *Seismic Performance Assessment of Buildings*, FEMA P-58, Applied Technology Council, Redwood City, CA, prepared for the Federal Emergency Management Agency, Washington, DC.

Anderson, T.L. (1995), *Fracture Mechanics*, 2nd Ed., CRC Press, Boca Raton, FL.

ASTM (2012), *Standard Specification for Through-Thickness Tension Testing of Steel Plates for Special Applications*, ASTM 770/A770M-03e1, ASTM International, West Conshohocken, PA.

AWS (2009), *Structural Welding Code—Seismic Supplement*, AWS D1.8/D1.8M: 2009, American Welding Society, Miami, FL.

AWS (2010), *Structural Welding Code—Steel*, AWS D1.1/D1.1M: 2010, American Welding Society, Miami, FL.

Barsom, J.M. and Rolfe, S.T. (1969), "Correlations between KIC and Charpy V-Notch Test Results in the Transition-Temperature Range," *Impact Testing of Metals*, ASTM STP 466, pp. 281–302.

Barsom, J.M. and Rolfe, S.T. (1999), *Fracture and Fatigue Control in Structures: Applications of Fracture Mechanics* (MNL41), 3rd Ed., ASTM Press, West Conshohocken, PA.

Curwen, T. (2014), "Built to Defy Severe Quakes, the New Wilshire Grand Is Seismically Chic," *Los Angeles Times*, November 2, 2014.

Joseph, L.M. and Maranian, P.J. (2017), "Grand Performance," *Civil Engineering*, ASCE, October Edition, pp. 48–57.

Lei, W., Van, X. and Yao, M. (1993), "Numerical Analysis of Strain Rate Field below Notch Root of Charpy V-Notch Test Specimen under Impact Loading Condition," *Engineering Fracture Mechanics*, Vol. 46, No. 4, pp. 583–593.

Nieblas, G. (2014), "Reaching New Heights in Los Angeles," *Structure Magazine*, December 2014.

Paris, P. and Erdogan, F. (1963, December), “A Critical Analysis of Crack Propagation Laws,” *Journal of Basic Engineering*, ASME, Vol. 85, No. 4, pp. 268–280.

Rice, J.R. (1968), “A Path Independent Integral and the Approximate Analysis of Strain Concentrations for Notches and Cracks,” *Journal of Applied Mechanics*, Vol. 35, No. 2, pp. 379–386.

Rooke, D.P. and Cartwright, D.J. (1976), *Compendium of Stress Intensity Factors*, HMSO, London, UK.